


Evaluation of Hexagonal Multi-Shape, Multi-Axial Geogrids in Unsurfaced Road Applications

Transportation Research Record
1–12
© National Academy of Sciences:
Transportation Research Board 2022
Article reuse guidelines:
sagepub.com/journals-permissions
DOI: 10.1177/03611981211069941
journals.sagepub.com/home/trr


William Jeremy Robinson¹ , Mark H. Wayne² , and Prajwol Tamrakar²

Abstract

A full-scale unsurfaced test section was constructed to evaluate the performance of two recently developed innovative geogrids, referred to as NX-1 and NX-2, having a unique combination of hexagonal, trapezoidal, and triangular aperture shapes, rib aspect ratios greater than 1.0, and a coextruded, composite polymer sheet designed to improve aggregate and geogrid interaction. The test section consisted of a 25-cm-thick crushed aggregate surface layer placed over a weak clay subgrade. Simulated truck traffic was applied using a load cart outfitted with a single-axle dual-wheel truck gear. Rutting performance and instrumentation response data gathered from earth pressure cells and single-depth deflectometers were monitored at multiple traffic intervals. It was found that the geogrids improved rutting performance when compared with an unstabilized test item, and NX-1 was found to be the best performer of the two geogrids. Calculated traffic benefit ratios ranged from approximately 1.2 at low levels of rutting up to approximately 13.0 at higher levels of rutting. Instrumentation response data indicated that the geogrids reduced measured pressure and deflection near the surface of the subgrade layer. Pressure response data in the aggregate layer suggested that the geogrids redistributed applied pressure higher in the aggregate layer, effectively changing the measured stress profile with depth.

Keywords

infrastructure, geology and geoenvironmental engineering, geosynthetics, pavements, pavement structural testing and evaluation, test tracks, roadway design, low-volume roads, granular and gravel

According to the Bureau of Transportation Statistics (1), as of 2019, there were 1.2 million mi of unpaved public roads in the United States, accounting for nearly 30% of the total public road mileage. These roads typically are considered farm-to-market connectors and play an important role in industries such as forestry, mining, and agriculture. Thus, the performance of these roadways is important to local rural economies.

Geosynthetics have been successfully used in lower-volume, that is, unsurfaced roadway applications to improve rutting performance. However, a single geogrid index property or a combination of index properties, have not been found to adequately predict anticipated performance. Some, for instance, Webster (2), Berg et al. (3), Giroud and Han (4), and Tang et al. (5) among others, have suggested that geosynthetic properties such as aperture stability, modulus, tensile strength, or soil-geosynthetic interaction may be an indicator of

anticipated performance. However, none of these properties definitively predict performance. In fact, if one consults AASHTO R50 (6), the state DOT guidance for geosynthetic reinforcement of aggregate layers, it explicitly states that the benefit of geosynthetic reinforced pavements may not be determined theoretically, but that test sections should be used to determine the anticipated benefit. One method could be to include a stabilization geosynthetic in a public-use roadway application, where areas of roadway are constructed with and without a geosynthetic to facilitate performance comparison.

¹U.S. Army Engineer Research and Development Center, Vicksburg, MS
²Tensar International, Alpharetta, GA

Corresponding Author:

William Jeremy Robinson, Jeremy.Robinson@usace.army.mil

Practically, a field test section would provide an indication of performance under comparable traffic conditions. However, the quantification of applied traffic in a field application presents some difficulty. Various types of vehicle could be expected, ranging from passenger cars to fully loaded trucks. Without a relatively sophisticated means of counting different vehicle types or individual axle loads, applied traffic can only be estimated, at best. Conversely, an accelerated pavement test (APT) experiment is typically performed under controlled loading conditions where accurate counts of applied load cycles are maintained. Thus, as new geosynthetic products are developed, it is paramount that they be evaluated in full-scale pavement test studies, under controlled conditions, to understand potential performance improvements that could be gained.

Objectives and Scope

The objective of this research was to evaluate the performance of two newly developed geogrids with a unique aperture shape in an unsurfaced pavement application. Three test items, two stabilized with new multi-axial geogrids and one unstabilized control, were constructed in the U.S. Army Engineer Research and Development Center's (ERDC) accelerated pavement test facility and subjected to accelerated truck loading using one of ERDC's load carts. Pavement surface rutting and instrumentation response data were the primary performance metrics considered to evaluate the effect of geogrid inclusion.

Literature Review

Several studies have evaluated the inclusion of geogrid in low-volume road applications and found improvements in rutting performance. Góngora and Palmeira (7) presented the results of cyclic plate load tests conducted on unstabilized and geogrid stabilized unpaved roads. The tests were conducted in a large steel tank and consisted of 230 mm of either gravel or recycled rubble fill placed over a 4% California Bearing Ratio (CBR) subgrade. Three different geogrids were evaluated of varying aperture size and strength characteristics. Loading was applied via a 200-mm diameter steel plate connected to a hydraulic system that yielded a vertical stress of 560 kPa. Loading was applied until 25 mm of deformation occurred after which the surface was repaired by refilling the rutted area. This process was repeated two additional times for a total of three loading stages. The results indicated that geogrid inclusion increased the number of load repetitions applied to the test items and was found to be beneficial after two rut repairs. Geogrid damage was observed in

the lighter duty geogrids in the last loading stage and was attributed to the coarse nature of the fill materials.

Kwon et al. (8) investigated the effect of geogrid reinforcement in full-scale low-volume surfaced road applications. The full-scale test section consisted of two asphalt layer thicknesses, that is, 76 and 127 mm, and three base layer thicknesses, that is, 203, 305, and 457 mm. The test items were trafficked using an ATLAS device outfitted with a dual-truck-tire assembly that had a total load of 44 kN, a speed of 8 km/h, and a tire inflation pressure of 690 kPa. Geogrids were placed at the subgrade-base interface as well as 152 mm from the top of the base. The results indicated that all reinforced pavement sections had better rutting performance than the unreinforced control sections. It was found that the geogrids reduced lateral movement of the aggregate which was confirmed by post-test forensic profiles.

Tingle and Jersey (9) evaluated the performance of eight full-scale aggregate road sections that included three different aggregate materials (crushed limestone, crushed chert gravel, and rounded clay gravel). Three of the eight 152 mm thick aggregate road sections were unreinforced (control) sections for each aggregate type. Geosynthetics included in the study consisted of a punched and drawn biaxial geogrid and a needle-punched nonwoven polypropylene geotextile. All sections were constructed over a 4 CBR clay subgrade. The test sections were trafficked with a dual-wheel tandem axle truck having a total gross weight of 194 kN and a tire contact pressure of 344 kPa. Results indicated that reinforced pavement sections displayed improved rutting resistance when compared with unreinforced sections for all aggregate types tested. The clay gravel was found to be the best performer, followed by the crushed limestone, and finally the crushed chert gravel. The authors attributed the clay gravel section's improved performance to natural cementation stemming from drying of the clay gravel base, noting that moisture susceptibility was not a test variable. It was found that the geogrid-reinforced crushed limestone section outperformed the geotextile-reinforced crushed limestone section, whereas the geotextile- and geogrid-reinforced crushed limestone section performed the best overall.

Wu et al. (10) evaluated the performance of geogrids in unbound aggregate layers using a small-scale loaded wheel tester and cyclic plate load test. For the loaded wheel test, specimens were prepared in a 600 mm × 400 mm × 100 mm test box, and load was applied using an Asphalt Pavement Analyzer (APA), which used three inflated rubber hoses and three steel wheels, and has typically been used for rutting evaluation of asphalt mixtures. The same size test box was used to prepare specimens for the cyclic plate test, and load was applied to a 165-mm diameter plate with a Material Testing and Simulation

(MTS) system. Two base course types were evaluated, that is, gravel and river sand, as well as four geogrids. The test results showed that the geogrids improved rutting resistance in both aggregate types, and it was found that the APA test results were capable of identifying the influence of geogrid aperture size and aggregate size on reinforcement effects.

Keller (11) summarized geosynthetic use by the United States Department of Agriculture's Forest Service in low-volume and rural road applications. The summary included a wide range of geosynthetic use ranging from drainage, retaining structures, and slope stabilization, as well as roadway reinforcement and stabilization. Of particular interest to this paper is the application of geosynthetics as a means to improve soft soil conditions in a roadway or access road application. It was noted that geotextiles had been used as a means to improve logging access roads since the 1970s. Further, it was noted that geogrids can provide a cost-effective repair approach for areas where settlement occurs along the uncompacted shoulder of a low-volume road.

A brief literature review suggested that geogrids have been shown to improve rutting performance in low-volume road applications over relatively soft subgrade soil support conditions. However, geogrid characteristics, that is, aperture size, shape, and so forth, have been shown to affect pavement performance. Thus, as new prototype geogrid products are developed that have unique aperture shapes and sizes, full-scale evaluations are desirable to determine performance improvement properties.

Test Section Properties

A full-scale test section consisting of three individual test items was constructed under shelter in ERDC's Hanger 2 Pavement Test Facility. Construction in a covered test facility minimized changes in material moisture content that could occur as a result of adverse weather events such as rainfall. Each test item was 3.8 m wide by 9.1 m long and consisted of a 25-cm-thick aggregate layer placed over a 61-cm-thick soft subgrade. Items 1 and 2 included a new multi-axial geogrid at the aggregate-subgrade interface, and Item 3 was an unstabilized control test item.

Test Item Material Properties

A high-plasticity clay, locally available in the Vicksburg area, was used to construct the subgrade layer. This material has been found to be advantageous for test section construction, primarily for its ability to maintain moisture content and design strength for the duration of a test. The high-plasticity clay had a liquid limit (LL) of

85, a plastic limit (PL) of 29, and a plasticity index (PI) of 56. An in-place CBR of 2% was targeted for construction and the results of laboratory CBR tests indicated that the targeted CBR could be achieved at an in-place moisture content of approximately 40%. Maximum dry density (MDD) was 1,699 kg/m³ at an optimum moisture content (OMC) of 19.7% according to modified proctor compaction procedures.

The aggregate layer was constructed with a crushed limestone material that had 67% gravel, 26% sand, and 8.5% fines passing a 0.075 mm sieve. The crushed limestone material had a 38 mm maximum aggregate size, an MDD of 2,369 kg/m³, and an OMC of 5.2% according to modified proctor compaction procedures. The aggregate layer was placed and compacted in one lift to mimic typical construction practices over extremely soft subgrades where the primary purpose is to bridge over the soft layer to mitigate the potential for pumping in the aggregate layer.

Geogrids evaluated in this study were manufactured from a coextruded, composite polymer sheet, which was then punched and oriented. The resulting structure consisted of continuous and non-continuous ribs forming three aperture geometries: hexagon, trapezoid, and triangle. The geogrids had differing aperture sizes allowing for interlock with a variety of aggregate sizes. The geogrids were designated as NX-1 and NX-2. NX-1 had a nominal node thickness of 5.5 mm and NX-2 had a nominal node thickness of 3.5 mm. Further NX-1 had a larger rib width and rib height than NX-2. In general, NX-1 was stiffer than NX-2. Both geogrids had a rectangular rib shape, a continuous parallel rib pitch of 80 mm, and a rib aspect ratio greater than 1.0. Photographs of the geogrids are shown in Figure 1.

Quality control tests were conducted during construction to verify that targeted material properties were achieved and to monitor material consistency. A summary of average as-constructed properties and measurement standard deviation are shown in Table 1.

As-built properties should be evaluated to identify potential differences in test item construction that could influence performance outcomes. A review of key subgrade construction characteristics suggests that the three test items had similar properties. Average dry density ranged from 1,318 to 1,337 kg/m³. Average oven-dried moisture contents, as well as CBR, were nearly identical for all test items, suggesting that any observed performance differences could be attributed to geosynthetic inclusion rather than differences in subgrade construction.

A review of aggregate surface properties indicated that dry density was the highest in Item 1, which contained NX-1, followed by Item 2, which contained NX-2, and finally the unstabilized control. This may suggest that NX-1, which had the largest rib width and rib height,

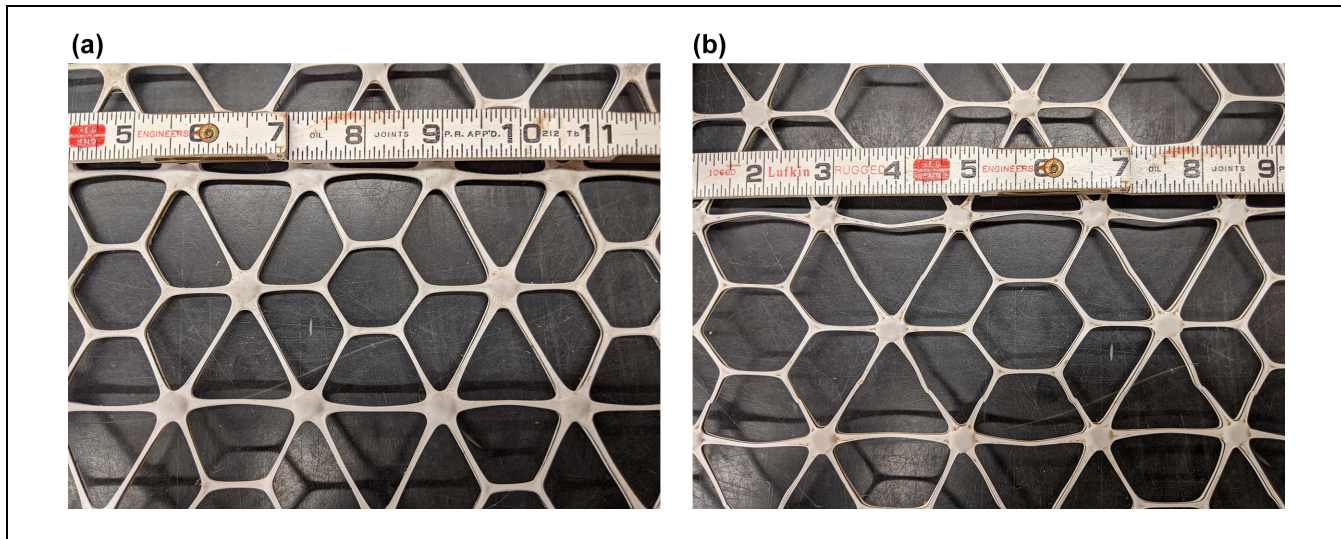


Figure 1. Photographs of prototype geogrids: (a) NX-1; and (b) NX-2.

Table 1. Summary of As-Built Properties

Property	n	Item 1 (NX-1)	Item 2 (NX-2)	Item 3 (Control)
Subgrade (MDD = 1,699 kg/m ³ @ OMC = 17.1%) ^a				
Dry density (kg/m ³)	24	1,337 ± 32	1,323 ± 43	1,318 ± 30
Nuclear moisture content (%)	24	33.8 ± 2.6	36.5 ± 3.2	37.2 ± 3.1
Compaction (%)	24	78.7	77.9	77.6
Oven-dried moisture (%)	24	40.4 ± 1.6	40.7 ± 1.5	40.6 ± 1.6
In-place CBR (%)	24	2.0 ± 0.3	2.0 ± 0.3	2.1 ± 0.3
Aggregate surface (MDD = 2,369 kg/m ³ @ OMC = 5.2%) ^a				
Dry density (kg/m ³)	6	2,267 ± 30	2,215 ± 27	2,202 ± 40
Nuclear moisture content (%)	6	4.3 ± 0.4	3.8 ± 0.2	3.7 ± 0.3
Compaction (%)	6	95.7	93.5	93.0
Oven-dried moisture (%)	6	2.9 ± 0.2	2.8 ± 0.3	3.2 ± 0.4
In-place CBR (%)	6	52.0 ± 3.0	47.3 ± 5.3	52.3 ± 11.8
Thickness (cm)	30	26.2 ± 1.0	27.2 ± 0.5	27.7 ± 0.5

Note: n = number of observations made to determine average; MDD = maximum dry density; OMC = optimum moisture content; CBR = California bearing ratio.

^aMaximum dry density and optimum moisture content as determined from ASTM D1557.

improved compactability of the aggregate layer, as all test items received the same level of compactive effort at the same time. Compaction in Item 1 was 95.7% of modified proctor, and Items 2 and 3 were generally 93% of modified proctor. Differences in final average compacted thickness of the aggregate layer were 1.5 cm. The aggregate layer contained up to 3.8 cm maximum aggregate size material. It was thus attempted to limit differences in aggregate layer thickness to half the maximum aggregate size or, in this case, 1.9 cm. The unstabilized item, Item 3, had the thickest average aggregate layer (27.7 cm), when compared with Item 1 (26.2 cm) and Item 2 (27.2 cm). Average aggregate CBR values were approximately 50, and it is noted that this material type typically yields CBRs in the order of 80–100 when placed in multiple 15- to 20-cm lifts. However, given the weakness of the

subgrade, the aggregate layer was placed in one single lift, simulating a typical construction practice of bridging over soft material to reduce subgrade pumping. Notably, variability—that is, standard deviation—in the measured CBR values was lowest in Item 1 that contained NX-1. Item 3 had the most variability, suggesting that the geogrids improved the uniformity of the measured CBR values, which tends to agree with compaction observations.

Load Cart Configuration

Simulated truck traffic was applied by using one of ERDC's load carts (Figure 2a) outfitted with a single-axle dual-wheel tire configuration (Figure 2b) mounted to a steel frame that was loaded with a series of cast lead weights to achieve the target load. The target total load

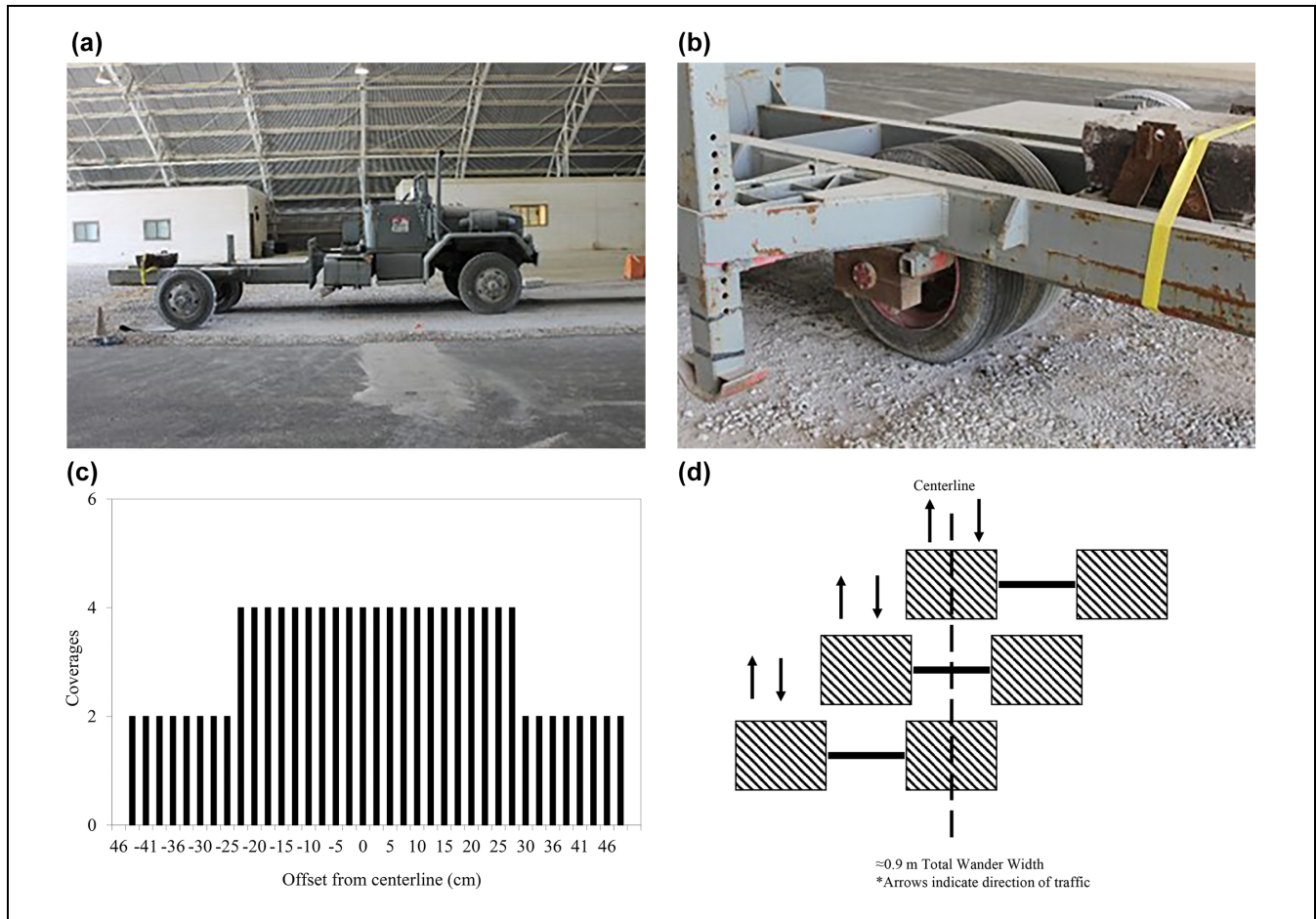


Figure 2. Traffic application equipment and traffic pattern: (a) overall view of U.S. Army Engineer Research and Development Center's (ERDC) load cart; (b) close-up of test gear configuration; (c) normally distributed pattern; and (d) traffic application pattern.

was 44 kN, that is, 22 kN per tire, and the tire inflation pressure was 827 kPa. After loading the test cart with lead weights, mobile aircraft scales were used to verify total load, and it was found that a total load of 46.1 kN was achieved, representing 1.05 times the targeted load.

A normally distributed traffic pattern (Figure 2c) with a total wander width of approximately 0.9 m was used to apply test traffic. Traffic was applied bi-directionally, where one pass was advanced forward in the selected position and the return pass was applied in the same selected position (Figure 2d). Test tire position was maneuvered in overrun areas to minimize impacts to the test area attributed to side shifting the load frame.

Instrumentation

Sensors were installed in the subgrade and aggregate layer to monitor pavement response during trafficking and to inform the effects of geogrid inclusion. Vertical stresses were measured using 22.9-cm-diameter earth pressure cells (EPC) that were installed near the surface

of the subgrade and near the bottom and mid-depth of the aggregate layer. EPCs installed in the subgrade had a maximum measurement range of 700 kPa, and EPCs installed in the aggregate layer had a maximum measurement range of 1 MPa. Vertical deflections in the subgrade were measured using single-depth deflectometers (SDD) installed near the surface of the subgrade. The SDD consisted of a linear variable differential transformer (LVDT) that was secured to a steel plate embedded near the top of the subgrade. The tip of the LVDT was positioned over a pre-placed fixed anchor rod that was secured at a depth of approximately 2.4 m below the top of the subgrade. Thus, the LVDT measured movement of the subgrade relative to the fixed anchor rod. A schematic showing a profile view of the instrumentation installation depths is shown in Figure 3.

Results

Traffic was applied until 75 mm of surface rutting was observed, or 10,000 traffic passes were completed,

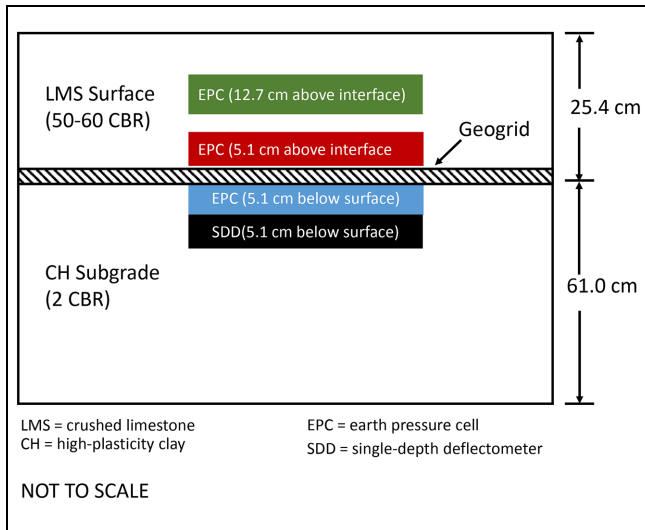


Figure 3. Profile view of instrumentation installation depth.
 Note: LMS = crushed limestone; EPC = earth pressure cells; SDD = single-depth deflectometers; CH = high-plasticity clay.

whichever occurred first. A 3.6-m-long straightedge was used to measure maximum rut depth at three equally spaced measurement locations in each test item, and average measurements were recorded. Rutting for this experiment included both permanent deformation in the wheel path and upheaval outside the wheelpath.

A statistical analysis was performed for each performance metric to determine if observed differences were statistically significant. A paired t-test was used for the analysis because test traffic was applied to all items simultaneously, data collection points were located at the same intervals, and all items were constructed at the same time using the same construction techniques. The t-test was evaluated at $\alpha = 0.05$ and a two-tailed rejection

region was considered, that is, the average difference between the observed values equaled zero.

Rutting

Measured rut depth with increasing traffic level is presented in Figure 4a. Rutting performance was generally equivalent up to approximately 400 passes, that is, about 6 mm rutting, suggesting that there was a period of initial shakedown or densification in the aggregate layer. After approximately 400 passes, it was observed that rutting performance began to diverge. Item 1 had the best rutting performance followed by Item 2. Rutting performance improvement in Item 1 could be attributed to the larger rib width and rib height of NX-1. Item 3 was the worst performer, as expected, and had approximately 12 mm more rutting at 2,000 passes. At the completion of trafficking, Item 3 had 45.7 mm more rutting than Item 1 and 35.6 mm more rutting than Item 2. Thus, the inclusion of geogrids dramatically improved rutting performance under the conditions of this study.

Permanent surface deformation, that is, change in elevation in the wheelpath, was measured using a robotic total station. Permanent surface deformation with traffic is presented in Figure 4b. Comparable to rutting performance, generally similar behavior was observed up to 400 passes. Differences in permanent deformation became evident after 400 passes, and Item 3 had more permanent deformation than Items 1 and 2. The difference in measured rut depth and permanent deformation gives an indication of the amount of aggregate upheaval, that is, shear flow, occurring in the aggregate layer. It was observed that the test items containing geogrids had little measured upheaval outside the wheel path, suggesting that the geogrids improved the overall stability of the

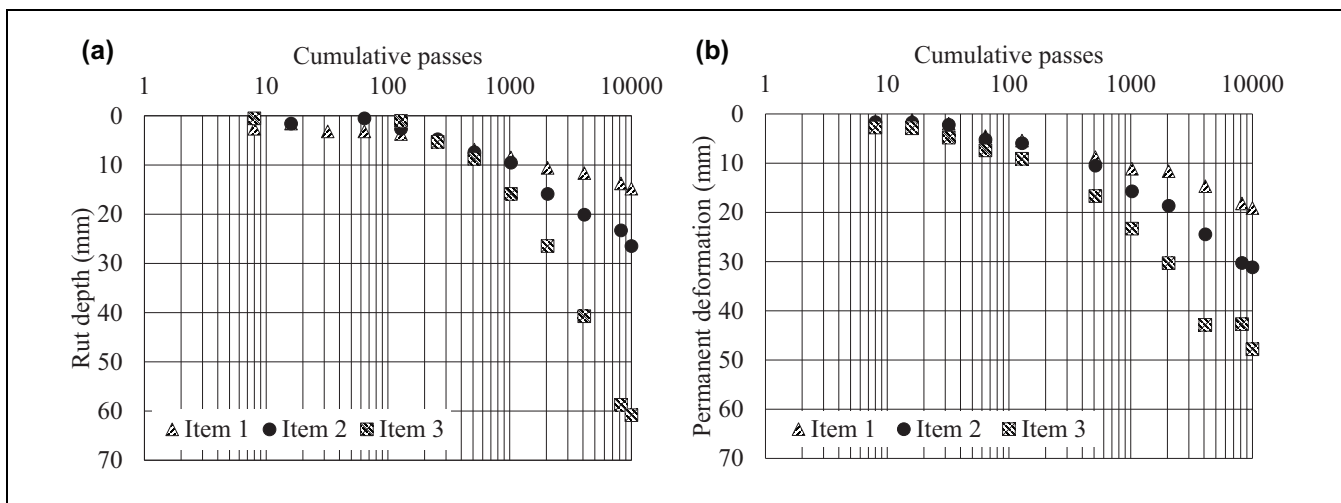


Figure 4. Measured rutting and surface deformation with traffic: (a) rut depth; and (b) permanent surface deformation.

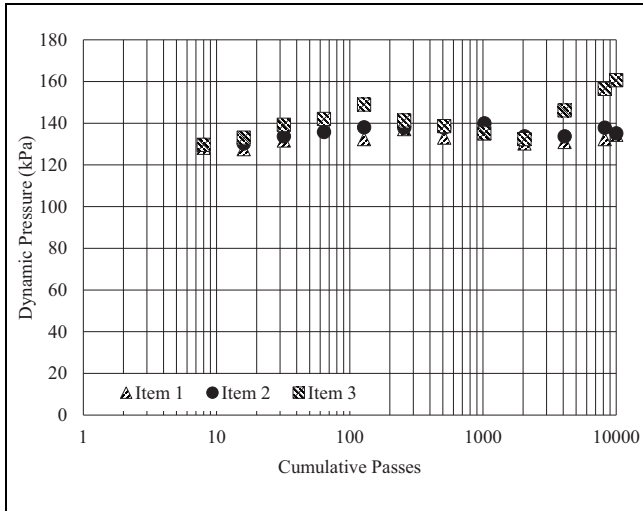


Figure 5. Subgrade pressure response with traffic.

aggregate layer. Item 3 had a meaningful amount of upheaval outside the wheel path of approximately 20 mm at the completion of trafficking.

Visual inspection revealed that a meaningful amount of pumping, that is, instability, was observed in Item 3 during traffic application. Items 1 and 2 generally appeared more stable, with minor pumping observed during traffic application. Thus, the improved stability attributed to geogrid inclusion observed in both rutting and permanent deformation data were confirmed by visual observation.

Subgrade Pressure Response

Representative pressure response values were determined by selecting the highest measured value near the end of a

selected traffic interval. Thus, the values selected represent a “best hit,” when the test gear was directly over an EPC. Response values were calculated by subtracting the peak value from the minimum value for the event, thus reported values represent maximum dynamic measurements. Maximum subgrade pressure response measurements are presented in Figure 5.

Maximum measured subgrade pressure was relatively consistent over the duration of test traffic, and a slight increase was observed early in traffic, that is, up to approximately 100 passes. Item 3 had a marginally higher measured subgrade pressure than Item 1, an average 6.8% increase, and Item 2 an average 4.9% increase, for a majority of traffic applications. A more definitive increase in subgrade pressure in Item 3, when compared with Item 1 with a 15.7% increase, and Item 2 with a 13.9% increase, was observed near the final data collection points. These observations suggest that the geogrids effectively reduced measured pressure on the subgrade, particularly at higher levels of surface deformation.

Aggregate Pressure Response

Representative aggregate pressure response values were selected using the same methodology as that described for the subgrade pressure response. The “best hit” was selected and the reported values represent the peak dynamic response measured during a selected traffic interval. Maximum aggregate response measured mid-depth (MD) of the aggregate layer is shown in Figure 6a.

Aggregate pressure response at mid-depth of the aggregate layer was found to be generally consistent throughout most of the traffic application. Similar to measured subgrade response values, an increase in MD aggregate pressure response was observed at the last two

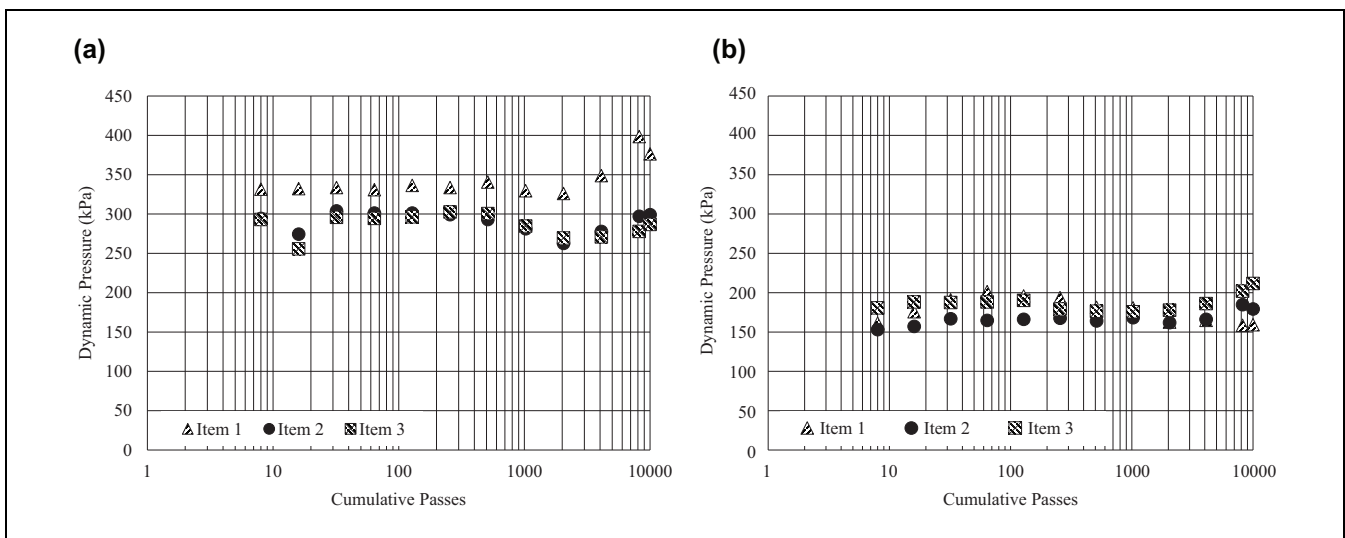


Figure 6. Aggregate pressure response with traffic: (a) mid-depth pressure response; and (b) bottom pressure response.

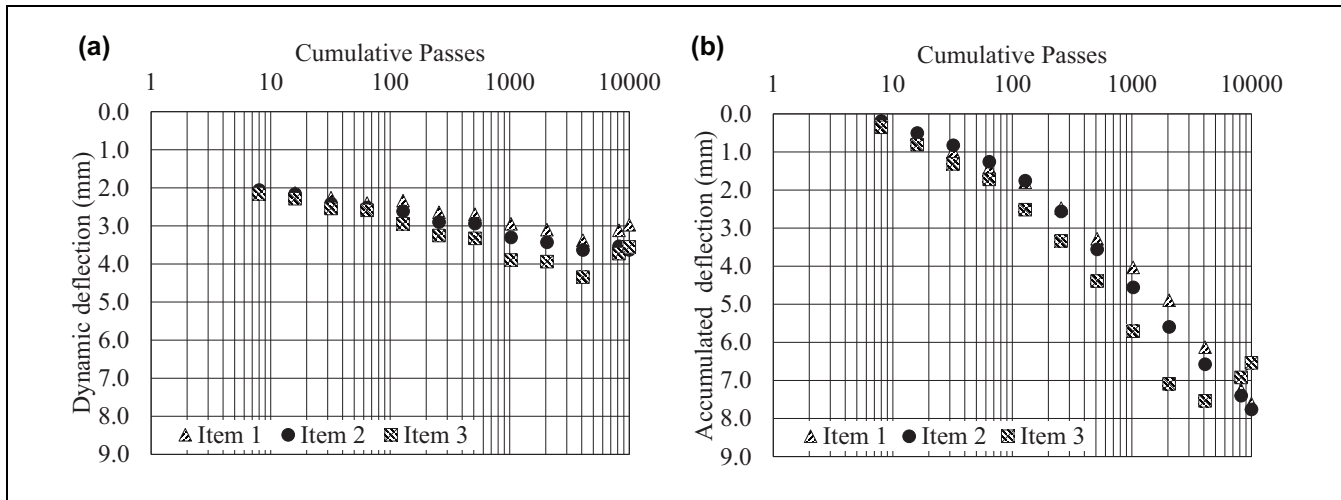


Figure 7. Single-depth deflectometers deflection response with traffic: (a) dynamic deflection; and (b) accumulated deflection.

data collection intervals. Higher MD base response values were observed in Item 1 when compared with Items 2 and 3 over the duration of traffic application. On average, MD base pressure in Item 1 was 15.5% higher than in Item 2 and 16.9% higher than in Item 3, which may be attributed to stiffening of the aggregate layer from geogrid inclusion. Thus, the stiffened aggregate layer appeared to redistribute applied pressure higher in the pavement structure, which agreed with observed reductions in measured subgrade pressure. Differences in measured values were not as dramatic in Items 2 and 3; in Item 2, the measured MD aggregate pressure was, on average, 1.7% higher than in Item 3.

Aggregate pressure response near the bottom of the aggregate layer is presented in Figure 6b. A slight increase in measured pressure was observed in all test items early in traffic, that is, up to approximately 100 passes, which agreed with other EPC measurements. Thereafter, Items 2 and 3 remained somewhat consistent for a majority of the test. Item 1 trended downward after reaching an early peak, suggesting that the geogrid was effective in reducing pressure with increasing traffic. On average, measured pressure in Item 3 was 5.2% higher than in Item 1 and 10.7% higher than in Item 2. Thus, both geogrids appeared to be effective in reducing measured pressure near the bottom of the aggregate layer.

Single-Depth Deflectometer Response

Single-depth deflectometer response measurements were analyzed to determine dynamic and accumulated deflections. Dynamic deflection measurements considered only the response from the tires moving over each sensor, and included the difference in local minimum and maximum values for each event. Accumulated deflections

considered the shift in initial baseline from the beginning of traffic, that is, pass zero, to the baseline at the end of each data collection point. Thus, accumulated deflection values represent permanent deformation near the top of the subgrade.

Measured dynamic deflections are presented in Figure 7a. Dynamic deflection tended to be similar for all three test items up to approximately 100 passes, after which performance differences began to emerge. Item 3 was observed to have the highest dynamic subgrade deflection, which was expected because of the lack of geogrid inclusion. Item 2, which contained NX-2, had slightly lower dynamic deflection than Item 3. Item 1, which contained NX-1, had the least measured dynamic subgrade deflection. Dynamic subgrade deflection in Item 1 was an average of 20.0% less than in Item 3, and 9.5% less than in Item 2. Item 2 dynamic deflections were approximately 9.6% less than Item 3. Percentage reductions were similar to observed reductions in measured subgrade pressure, reinforcing the proposition that the geogrids were successful in protecting the subgrade.

Measured accumulated deflections for each test item (Figure 7b) showed similar trends. Item 3 had the highest accumulated subgrade deflection, followed by Items 2 and 1. Accumulated deflection in Item 1 was approximately 17.9% less than in Item 3 and approximately 4.5% less than in Item 2. Item 2 accumulated deflection was approximately 12.9% less than Item 3. Thus, comparable to dynamic deflection, it could be suggested that the geogrids were effective in reducing long-term permanent deflection, that is, damage, of the subgrade layer.

It should be noted that a relatively sharp decrease in dynamic SDD response was observed in Items 1 and 3 after approximately 4,000 passes and was unexpected. A review of the Item 1 response signal did not suggest that

Table 2. Summary of Statistical Analysis

Interaction	n	p-Value	Significant	Better performer
Rut depth				
Item 1 versus Item 2	8	0.043	Yes	Item 1
Item 1 versus Item 3	8	0.039	Yes	Item 1
Item 2 versus Item 3	8	0.039	Yes	Item 2
Surface deformation				
Item 1 versus Item 2	12	0.010	Yes	Item 1
Item 1 versus Item 3	12	0.008	Yes	Item 1
Item 2 versus Item 3	12	0.007	Yes	Item 2
Subgrade pressure				
Item 1 versus Item 2	12	0.003	Yes	Item 1
Item 1 versus Item 3	12	0.004	Yes	Item 1
Item 2 versus Item 3	12	0.024	Yes	Item 2
Aggregate pressure—mid-depth				
Item 1 versus Item 2	12	<0.001	Yes	Item 1
Item 1 versus Item 3	12	<0.001	Yes	Item 1
Item 2 versus Item 3	12	0.098	No	Same
Aggregate pressure—bottom				
Item 1 versus Item 2	12	0.086	No	Same
Item 1 versus Item 3	12	0.144	No	Same
Item 2 versus Item 3	12	<0.001	Yes	Item 2
Dynamic deflection				
Item 1 versus Item 2	12	0.001	Yes	Item 1
Item 1 versus Item 3	12	<0.001	Yes	Item 1
Item 2 versus Item 3	12	0.002	Yes	Item 2
Accumulated deflection				
Item 1 versus Item 2	12	0.099	No	Same
Item 1 versus Item 3	12	0.035	Yes	Item 1
Item 2 versus Item 3	12	0.047	Yes	Item 2

a gauge malfunction occurred as a clear response with little electronic noise was observed. Additionally, a review of accumulated response data did not reveal a similar decrease, further suggesting the gauge was functioning properly. Comparatively, a meaningful increase in measured MD aggregate pressure response was observed during the same data collection interval. Coupling these observations suggests that an aggregate stiffness enhancement via improved aggregate interlock may have occurred thereby reducing the dynamic SDD response.

A review of the Item 3 response signal indicated that the gauge was functioning properly. Conversely to Item 1 observations, accumulated deflection values in Item 3 experienced a similar decrease in dynamic values. It is hypothesized that slippage occurred between the LVDT and the LVDT attachment flange that could explain changes in both dynamic and accumulated response values.

Statistical Analysis of Test Section Results

Table 2 contains the results of a statistical analysis performed on all measured pavement response values. It should be noted that a relatively small sample size was evaluated. However, all data collection points were

generally selected based on visual observation of rut depth development. Thus, it was necessary to balance data collection efforts with manpower efficiency, that is, test data were collected to capture meaningful changes in test item performance. A paired t-test indicated that none of the rut depth interactions were statistically significant, which was an unexpected result. However, a review of the data showed that very little rutting occurred early in traffic, that is, up to 128 passes, after which rutting began to develop. Thus, the differences at early data collection points were near zero, introducing bias in the statistical measure. When the analysis was conducted on data points after 128 passes, meaningful and expected statistical differences were observed. The analysis indicated that all comparisons were statistically significant, and that average rutting in Item 3 was more than average rutting in Items 1 and 2. Further, Item 1 was found to be statistically different from Item 2, and average rutting performance was found to be better in Item 1.

Permanent deformation comparisons were found to be statistically significant, indicating that average permanent deformation was different in all test items. Item 1 was found to have the lowest average permanent deformation. Item 2 was found to be the next best performer, followed by Item 3.

Table 3. Traffic Benefit Ratio

Performance	Test item	Rut depth			
		6.0 mm	12.7 mm	19.0 mm	25.4 mm
Passes to rut	Item 1 passes	427	6,144	15,800	25,300
	Item 2 passes	410	1,536	3,584	9,397
	Item 3 passes	334	795	1,331	1,946
Traffic benefit ratio	Item 1 TBR	1.3	7.7	11.9	13.0
	Item 2 TBR	1.2	1.9	2.7	4.8

Note: Bold font indicates extrapolated values. TBR = traffic benefit ratio.

All subgrade pressure interactions were found to be statistically significant, indicating that meaningful differences were observed. Item 1 was the best performer, having the lowest average subgrade pressure. Both geogrid stabilized items, that is, Items 1 and 2, had statistically lower average subgrade pressure than the unstabilized Item 3.

MD pressure in Item 1 was found to be statistically different from the other two test items, and Item 1 had a higher average MD base pressure in both cases. Statistical comparison of MD base pressure between Items 2 and 3 was not found to be statistically significant (p -value = 0.098).

A comparison between measured pressure near the bottom of the aggregate layer in Items 2 and 3 was found to be significant, and Item 2 had a lower average measured pressure near the bottom of the aggregate layer.

With regard to dynamic deflection, all comparisons were found to be statistically significant. Item 1 had lower average dynamic deflection than Items 2 and 3, which was expected given that Item 1 contained the stiffer geogrid. Item 2 had lower average dynamic deflection than Item 3. In accumulated deflection, the statistical analysis indicated that differences in the two geogrids were unremarkable. However, differences between the individual geogrid test items and the unstabilized test item were found to be statistically significant, suggesting that the geogrids were effective in reducing permanent deformation at the top of the subgrade.

Analysis of Test Results

Traffic Benefit Ratio

The traffic benefit ratio (TBR) has been used as a means of quantifying the performance improvement that could be gained from geogrid inclusion. Simply, the number of traffic passes of a geogrid stabilized pavement section is compared with the number of traffic passes of an unstabilized pavement section. For valid comparisons to be made, the pavement sections should have the same pavement thickness and cross-section properties.

Calculated TBR values at various rut depths are presented in Table 3. It should be noted that Item 1 did not exceed 19.0 mm of rutting in a reasonable amount of traffic passes. The numbers of passes to achieve 19.0 mm and 25.4 mm of rutting were thus estimated based on linear extrapolation from available data. Therefore, these TBR values should be considered approximations only. In both geogrid stabilized test cases, it was found that TBR increased with an increase in rut depth, suggesting that the geogrids were successful in stabilizing the aggregate layer. Higher TBR values were observed in Item 1, compared with Item 2, which could be attributed to the increased stiffness of NX-1. Meaningful improvements in both geogrid test items were observed at all rut depths.

It should be noted that the calculated TBR values are for unpaved sections under the conditions of this experiment. Different TBR values could be obtained in an experiment including a paved surface layer; thus the TBR values here should be used for comparison purposes only.

Equivalent Thickness Methodology

Early USACE geogrid design methodology has been implemented in ETL 1110-1-189: Use of Geogrids in Pavement Construction in the form of an equivalent pavement thickness chart that is generally considered valid for subgrade CBR values ranging from 0.5 to 8.0. Recently, Robinson et al. (12) updated the equivalent pavement thickness chart based on a comprehensive analysis that included a host of data collected since the initial development of the equivalent thickness chart. The equivalent thickness chart provides a means to evaluate improvements that could be gained from geogrid inclusion in aggregate thickness of an unstabilized pavement layer. It should be noted that the equivalent thickness chart was developed in U.S. customary units. All calculations were thus performed in U.S. customary units. Appropriate conversions to metric units for the purposes of this paper are provided.

An empirical relationship was developed between the applied equivalent single-axle loads (ESALs) at 1.0 in. of

Table 4. Summary of Equivalent Thickness Analysis

	Item 1	Item 2	Item 3
ESALs at 1.0 in. (25.4 mm)	38,000	14,190	2,938
Calculated thickness, in. (cm)	15.3 (38.9)	14.0 (35.6)	12.0 (30.5)
Normalized improvement, in. (cm)	3.3 (8.4)	2.0 (5.1)	na
Comparison to as-built thickness, in. (cm)	+5.0 (12.7)	+3.3 (8.4)	+1.1 (2.8)

Note: Bold font indicates extrapolated values. ESAL = equivalent single-axle load; na = not applicable.

rutting and the thickness of an equivalent geogrid stabilized aggregate layer. To determine an equivalent unstabilized aggregate layer thickness that yields the same performance of a thinner stabilized aggregate layer, the thickness chart can be entered using the applied ESALs from a geogrid stabilized pavement on the x-axis, intercepting the unstabilized regression line, and moving left to the aggregate thickness on the y-axis. As an alternative, the unstabilized regression equation could be used to calculate an equivalent thickness. In the case of this study, the applied ESALs to achieve 1 in. rutting can be used to calculate an equivalent thickness. Applied ESALs were calculated by multiplying traffic passes of the load cart by an equivalent single-axle load factor. In the case of this experiment, one pass of the load cart was equivalent to 1.51 ESALs (13).

Calculations were conducted for each test item using the relationship:

$$T = 1.300 * \ln(\text{ESALs}) + 1.6$$

where T = thickness of the aggregate layer (in.) and ESALs = total ESALs to achieve 1.0 in. of rutting. A summary of the calculations is provided in Table 4. The analysis indicated that the performance of Item 3 was equivalent to a 12-in.-thick aggregate layer and was approximately 1.1 in. greater than the as-built thickness. The calculated thickness of each stabilized test item was normalized to the calculated thickness of Item 3, and it was found that the inclusion of geogrid in Item 2 provided performance improvement equivalent to the addition of 2.0 in. of aggregate and that geogrid inclusion in Item 1 provided performance improvement equivalent to an additional 3.3 in. of aggregate. When the calculations are compared with the as-built thickness, it was found that Item 2 resulted in a 3.3-in. aggregate thickness increase and Item 1 resulted in a 5.0-in. aggregate thickness increase. Simply stated, the analysis indicated that the inclusion of a geogrid resulted in performance that would be expected from a thicker unstabilized pavement section. The analysis suggested that meaningful reductions in aggregate thickness could be achieved while maintaining similar performance as an unstabilized pavement layer.

Conclusions

A full-scale test section was constructed to evaluate the performance of multi-axial geogrids in an unsurfaced pavement structure. The construction and traffic data were analyzed to assess the performance of the new multi-axial geogrids relative to each other, as well as relative to an unstabilized control section. The test items were constructed and trafficked simultaneously allowing for a meaningful performance comparison. Analysis of the test results yielded the following conclusions.

1. As-built properties suggested that the multi-axial geogrids improved compaction and reduced compaction variability in the aggregate layer.
2. The inclusion of the multi-axial geogrids resulted in significant rutting resistance when compared with the unstabilized control test item. Further, upheaval outside the wheel path was less in the geogrid test items than the unstabilized control.
3. Item 1, which contained NX-1, was found to be the best rutting performer, and had approximately 15 mm of rutting at the conclusion of traffic. Item 2, which contained NX-2, was the next best performer and had 25 mm of rutting. By comparison, Item 3, the unstabilized control, had 61 mm of rutting at the conclusion of traffic.
4. Subgrade pressure response measurements indicated that geogrid inclusion provided minor pressure reductions early in traffic, but a more meaningful reduction, that is, in the order of 14% to 16%, were observed near the final data collection points. Thus, the data suggests that the geogrids were effective in reducing measured pressure on the subgrade.
5. Single-depth deflectometer measurements indicated that geogrid inclusion reduced dynamic deflection on the subgrade from 10% to 20%. Similar reductions were observed in accumulated, that is, permanent, deflection. Thus, the data suggest that the geogrids were effective in reducing measured deflection near the surface of the subgrade.
6. Measured MD aggregate pressure was found to be approximately 16% higher in the geogrid test

items when compared with the unstabilized control item. This suggests that geogrid inclusion stiffened the aggregate layer and resulted in a redistribution of applied pressure higher in the pavement structure.

7. Pressure measured at the bottom of the aggregate layer was found to be 5% to 10% lower in the geogrid test items when compared with the unstabilized control. These data agree with pressure measurements in the subgrade and support the hypothesis of a redistribution of applied pressure.

Author Contributions

The authors confirm contribution to the paper as follows: study conception and design: W. Jeremy Robinson, Mark H. Wayne, Prajwol Tamrakar; data collection: W. Jeremy Robinson; analysis and interpretation of results: W. Jeremy Robinson, Mark H. Wayne, Prajwol Tamrakar; draft manuscript preparation: W. Jeremy Robinson, Mark H. Wayne, Prajwol Tamrakar. All authors reviewed the results and approved the final version of the manuscript.

Declaration of Conflicting Interests


The author(s) declared no potential conflicts of interest with respect to the research, authorship, and/or publication of this article.

Funding

The author(s) disclosed receipt of the following financial support for the research, authorship, and/or publication of this article: The tests described and the resulting data presented here, unless otherwise noted, were obtained from research sponsored by Tensar International, and performed by the U.S. Army Engineer Research and Development Center. Permission was granted by the Director, Geotechnical and Structures Laboratory, and Tensar International to publish this information.

ORCID iDs

William Jeremy Robinson  <https://orcid.org/0000-0002-1175-0144>

Mark H. Wayne  <https://orcid.org/0000-0001-6474-3899>

References

1. Bureau of Transportation Statistics. Public Road and Street Mileage in the United States by Type of Surface. <https://www.bts.gov/content/public-road-and-street-mileage-united-states-type-surfacea>.
2. Webster, S. L. *Geogrid Reinforced Base Courses for Flexible Pavements for Light Aircraft: Test Section Construction, Behavior Under Traffic, Laboratory Tests, and Design Criteria*. No. WES/TR/GL-93-6. Geotechnical Laboratory, US Army Engineer Waterways Experiment Station, Vicksburg, MS, 1993.
3. Berg, R. R., B. R. Christopher, and S. W. Perkins. *Geosynthetic Reinforcement of the Aggregate Base Course of Flexible Pavement Structures*. GMA White Paper II. Geosynthetic Materials Association, Roseville, MN, 2000, p. 130.
4. Giroud, J. P., and J. Han. Design Method for Geogrid-Reinforced Unpaved Roads. I. Development of Design Method. *Journal of Geotechnical and Geoenvironmental Engineering*, Vol. 130, No. 8, 2004, pp. 775–786. [https://doi.org/10.1061/\(ASCE\)1090-0241\(2004\)130:8\(775\)](https://doi.org/10.1061/(ASCE)1090-0241(2004)130:8(775)).
5. Tang, X., G. R. Chehab, A. M. Palomino, S. R. Allen, and C. J. Sprague. Laboratory Study on Effects of Geogrid Properties on Subgrade Stabilization of Flexible Pavements. In *Proc., GeoCongress 2008: Geosustainability and Geohazard Mitigation* (K. R. Reddy, M. V. Khire, and A. N. Alshawabkeh, eds.), New Orleans, LA, March 9–12, 2008, American Society of Civil Engineers, Reston, VA, pp. 1089–1096.
6. AASHTO R50-09. *Recommended Practice for Geosynthetic Reinforcement of the Aggregate Base Course of Flexible Pavement Structures*. AASHTO, Washington D.C., 2018.
7. Góngora, I. A. G., and E. M. Palmeira. Influence of Fill and Geogrid Characteristics on the Performance of Unpaved Roads on Weak Subgrades. *Geosynthetics International*, Vol. 19, No. 2, 2012, pp. 191–199.
8. Kwon, J., E. Tutumluer, I. Al-Qadi, and S. Dessouky. Effectiveness of Geogrid Base-Reinforcement in Low-Volume Flexible Pavements. In *Proc., GeoCongress 2008: Geosustainability and Geohazard Mitigation* (Reddy, K. R., M. V. Khire, and A. N. Alshawabkeh, eds.), New Orleans, LA, March 9–12, 2008, American Society of Civil Engineers, Reston, VA, pp. 1057–1064.
9. Tingle, J. S., and S. R. Jersey. Full-Scale Evaluation of Geosynthetic-Reinforced Aggregate Roads. *Transportation Research Record: Journal of the Transportation Research Board*, 2009. 2116: 96–107.
10. Wu, H., B. Huang, X. Shu, and S. Zhao. Evaluation of Geogrid Reinforcement Effects on Unbound Granular Pavement Base Courses Using Loaded Wheel Tester. *Geotextiles and Geomembranes*, Vol. 43, No. 5, 2015, pp. 462–469.
11. Keller, G. R. Application of Geosynthetics on Low-Volume Roads. *Transportation Geotechnics*, Vol. 8, 2016, pp. 119–131.
12. Robinson, W. J., J. S. Tingle, G. J. Norwood, and I. L. Howard. Assessment of Equivalent Thickness Design Principles for Geosynthetic Reinforced Pavements by Way of Accelerated Testing. *Transportation Research Record: Journal of the Transportation Research Board*, 2018. 2672: 132–142.
13. Huang, Y. H. *Pavement Design and Analysis*. Pearson/Prentice Hall, Upper Saddle River, NJ, 2004.